High-terrain land surface temperature, circumpolar teleconnection aerosol-snow-darkening effect, and sub-seasonal to seasonal (S2S) global precipitation predictability

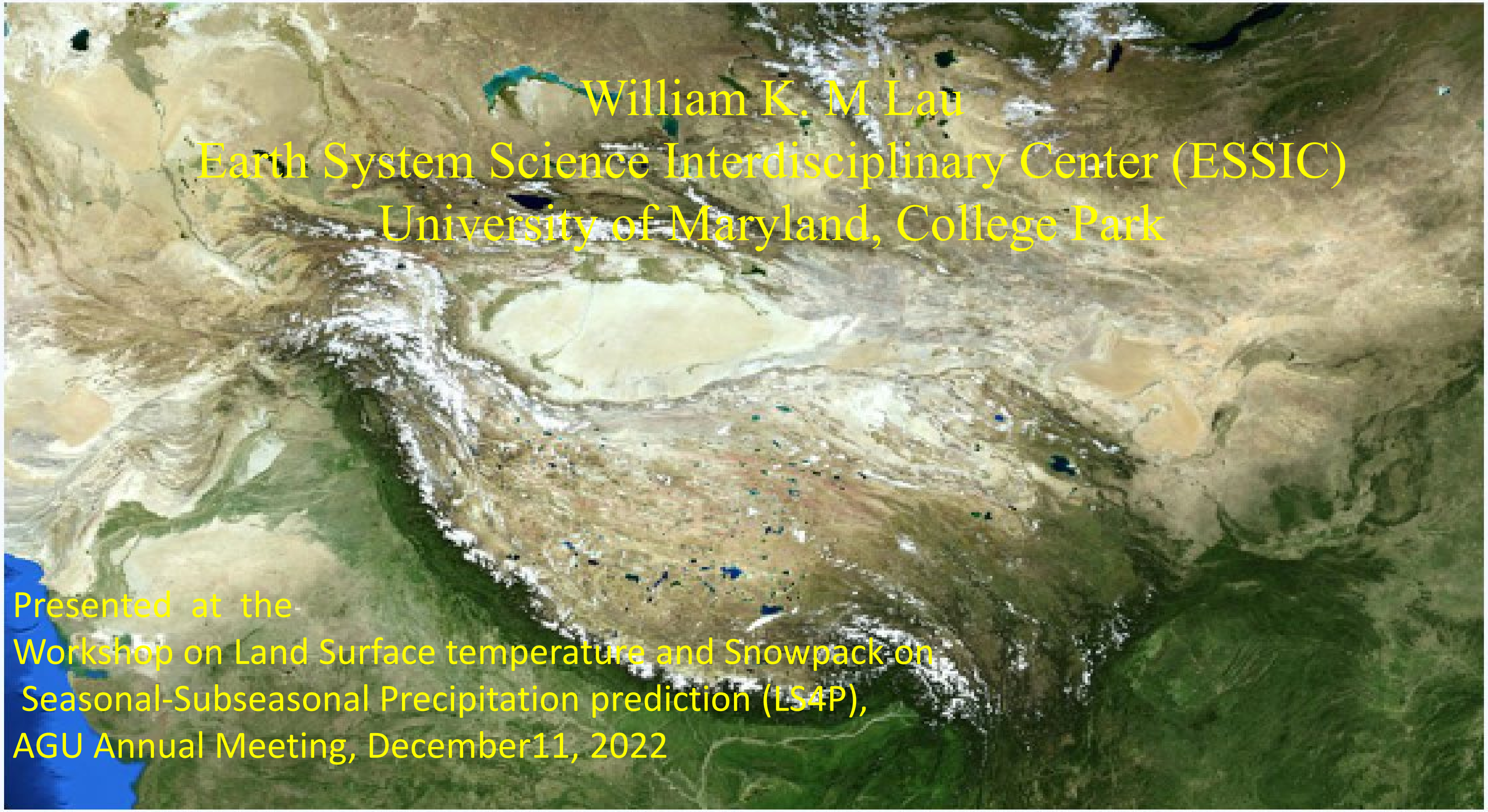

William K. M Lau
Earth System Science Interdisciplinary Center (ESSIC)
University of Maryland, College Park

Presented at the
Workshop on Land Surface temperature and Snowpack on
Seasonal-Subseasonal Precipitation prediction (LS4P),
AGU Annual Meeting, December11, 2022

2003 anomalous cold T2m over TP

Comparison of Observed and Simulated June 2003 Precipitation Anomaly

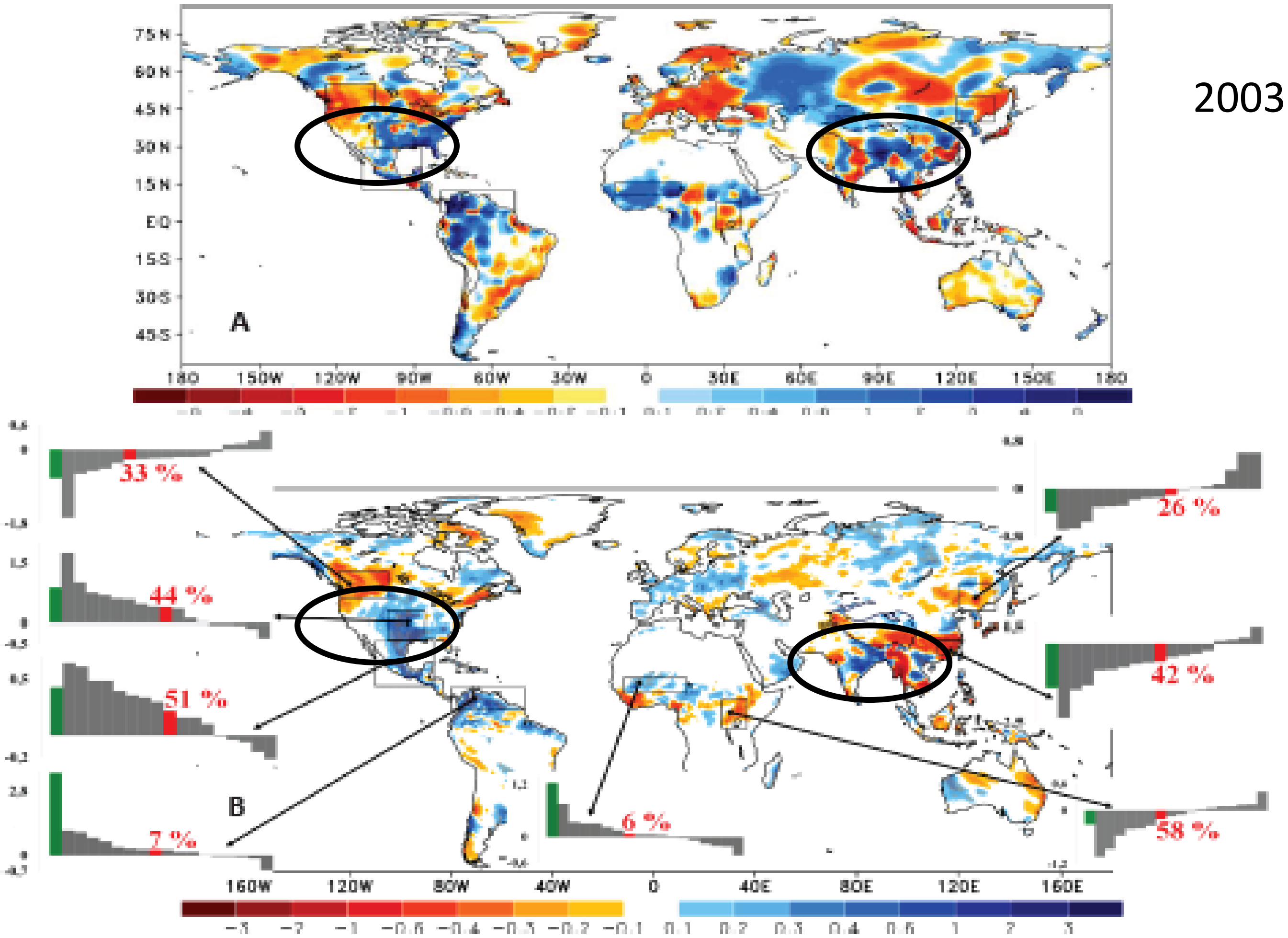

Fig. 3. Comparison of Observed and Simulated June 2003 Precipitation Anomaly. (A) Observed difference between year of 2003 and the mean of 1981-2010. **(B)** Model-simulated precipitation anomalies (mm/day) after producing the cold TP anomaly shown in Figure 2B. Notes: (1) Boxes indicate the hot spots; (2) Gray bars denote different models and are arranged in a descending order for each region; green bar is observation and red bar is ensemble mean in each hot spot; (3) Simulated percentages of observed anomalies from the ensemble mean are shown in red color above or below the red bars.

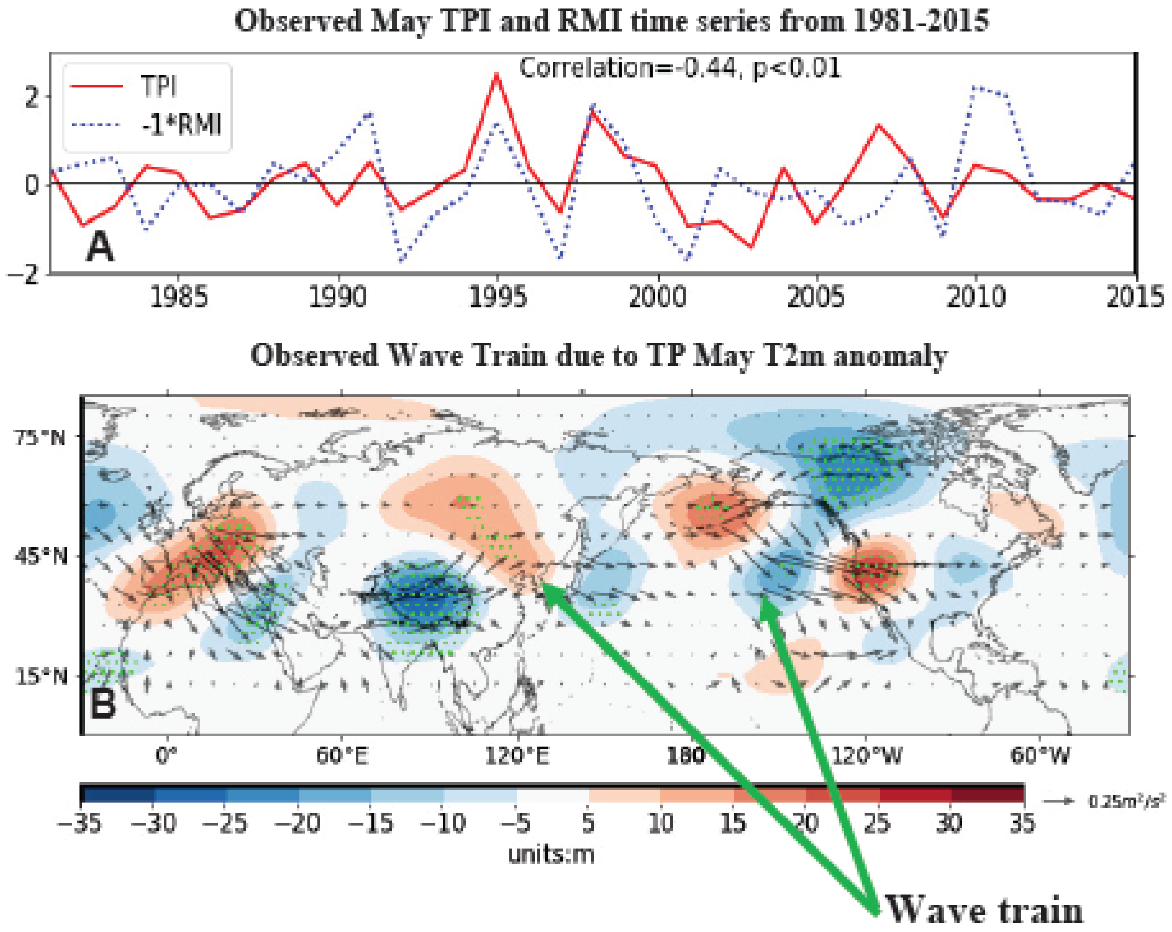

Fig. 4. Linkage between the TP and North America. (A) TPI and RMI time series. (B) Wave train. Notes: Fig. 4B is the regression of May 200-hPa geopotential height (m) of NCEP Reanalysis I from 1981-2015 onto (-1) * normalized May TPI and corresponding wave activity flux (WAF; m2/s2). Shadings denote the geopotential height, vectors denote the WAF.

T2m over Tibetan Plateau (TPI), Rocky Mt (RMI) respectively

200 hPa GPH anomalies
Regressed to TPI (1981-2015)

Day 2

Day 5

Day 10

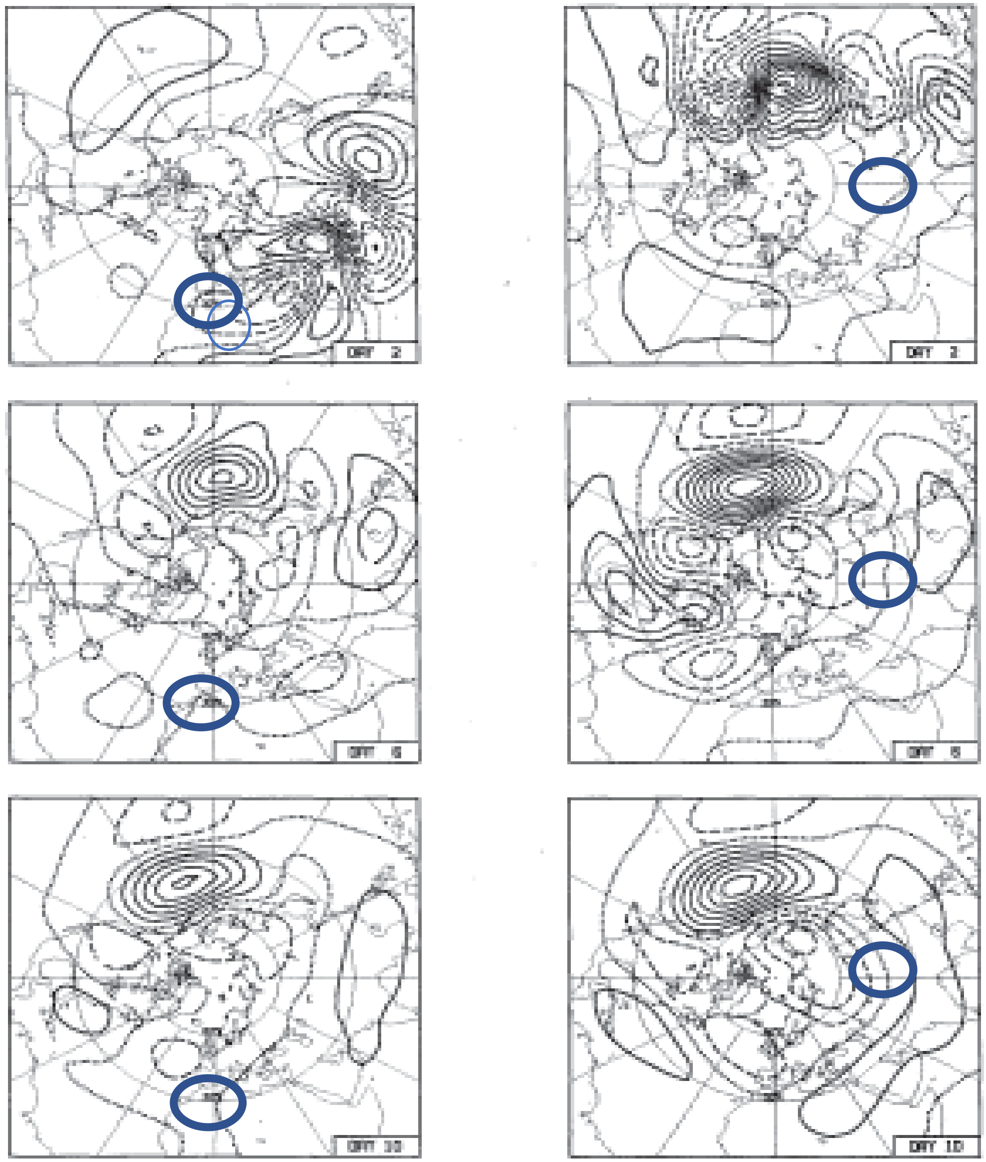

FIG. 6. The perturbation streamfunction at days 2, 5 and 10 for an initial negative disturbance centered at 30°N, 0°E. The contour interval is $^1/_{20}$ of the initial maximum amplitude. Positive contours are drawn with solid lines, negative contours with dashed lines, and the zero contour is dotted.

(30N, 0E)

FIG. 7. As in Fig. 6, but for an initial perturbation at 30°N, 120°E.

(30N, 120E)

Simmons, Wallace and Branstator, 1983, JAS

Energy dispersion via
Barotropic (same sign in vertical)
Instability of the mean midlatitude
westerly Jetstream during boreal winter

Lau and Peng (1992), dynamical model

FEBRUARY 1992 LAU AND PENG

Boreal summer (JJA) barotropic Steady state response somewhat independent of region of forcing

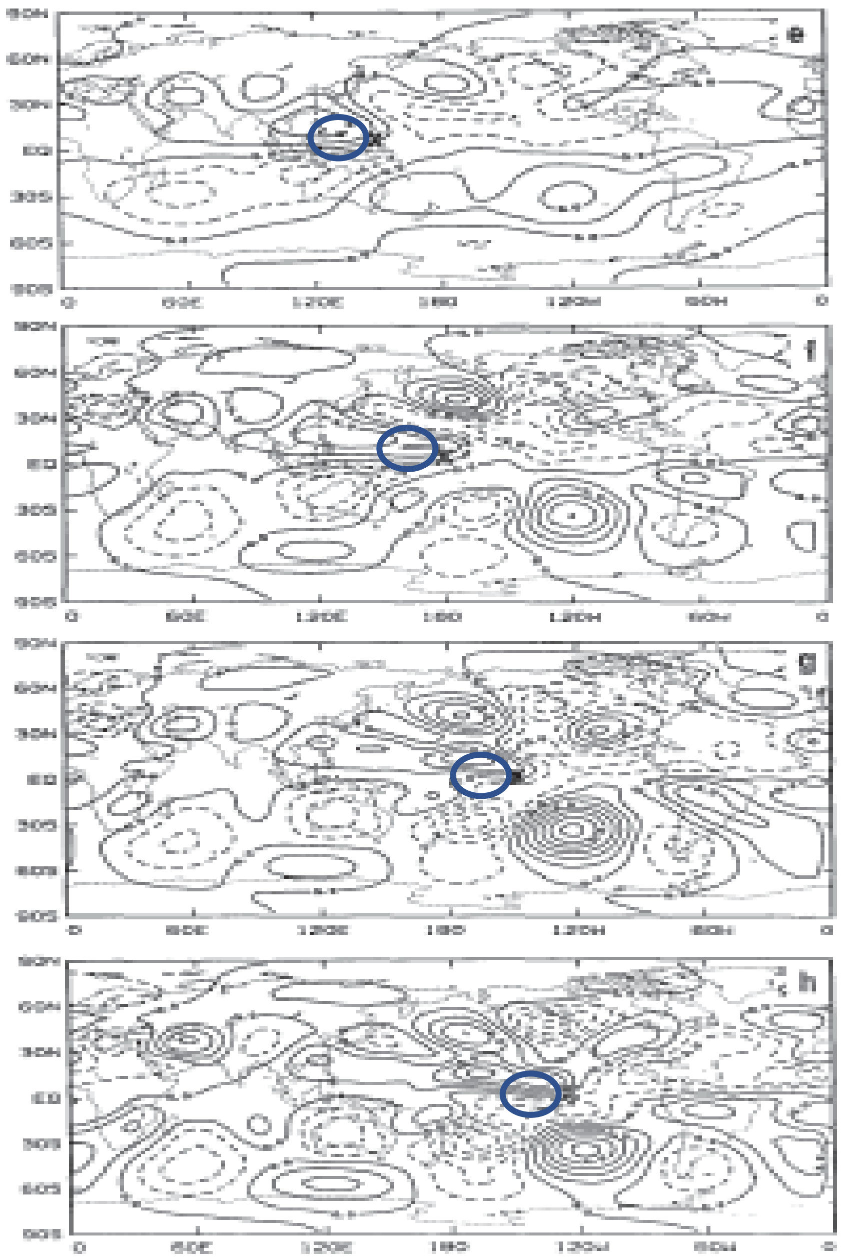

FIG. 11. (Continued) (e) 150°E, (f) 180°, (g) 150°W, and (h) 120°W. Contour interval for streamfunction is 2×10^6 m^2 s^{-1}.

Lau and Weng (2002), observations

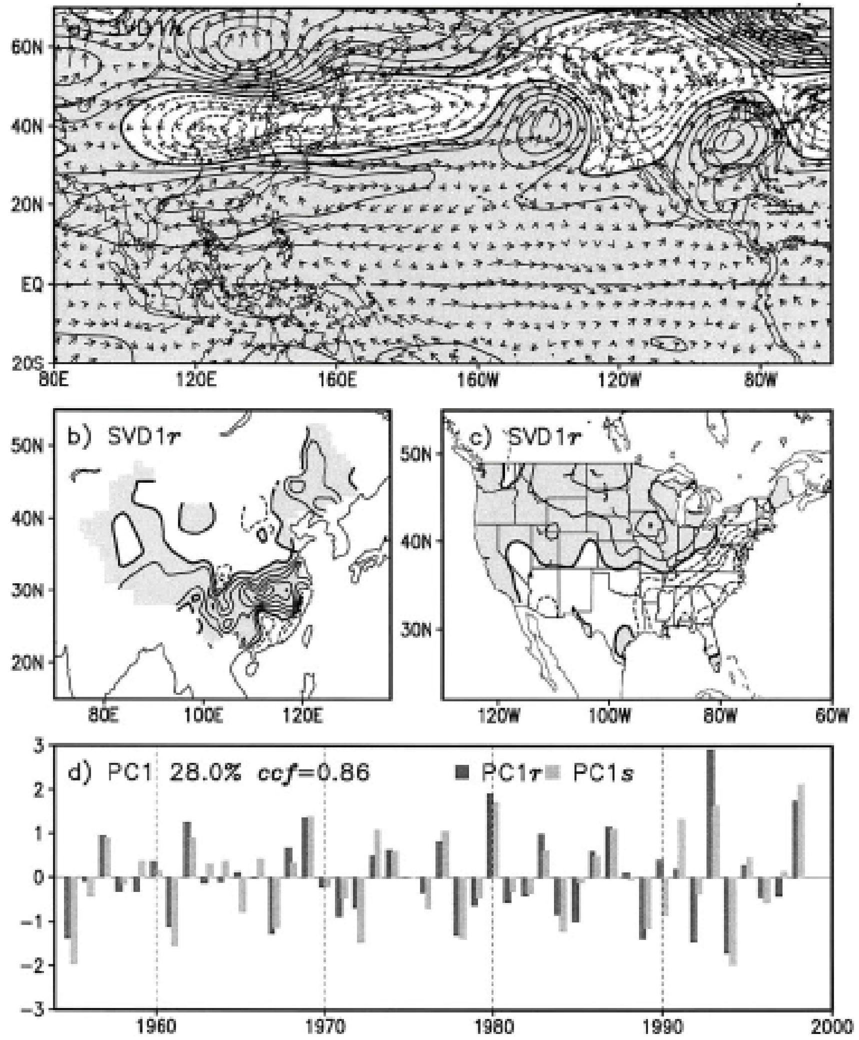

Fig. 6. SVD1 between 500 hPa geopotential height and combined US-China JJA normalized rainfall anomalies. The contour interval is 2 gpm in a), 20 mm in b) and 10 mm in c). The linear regression of 850 hPa wind against the rainfall PC is also shown in a). Speed less than 0.1 m/s is suppressed.

Circum-global-teleconnection (CGT)
In northern hemisphere summer (Ding and Wang 2005)

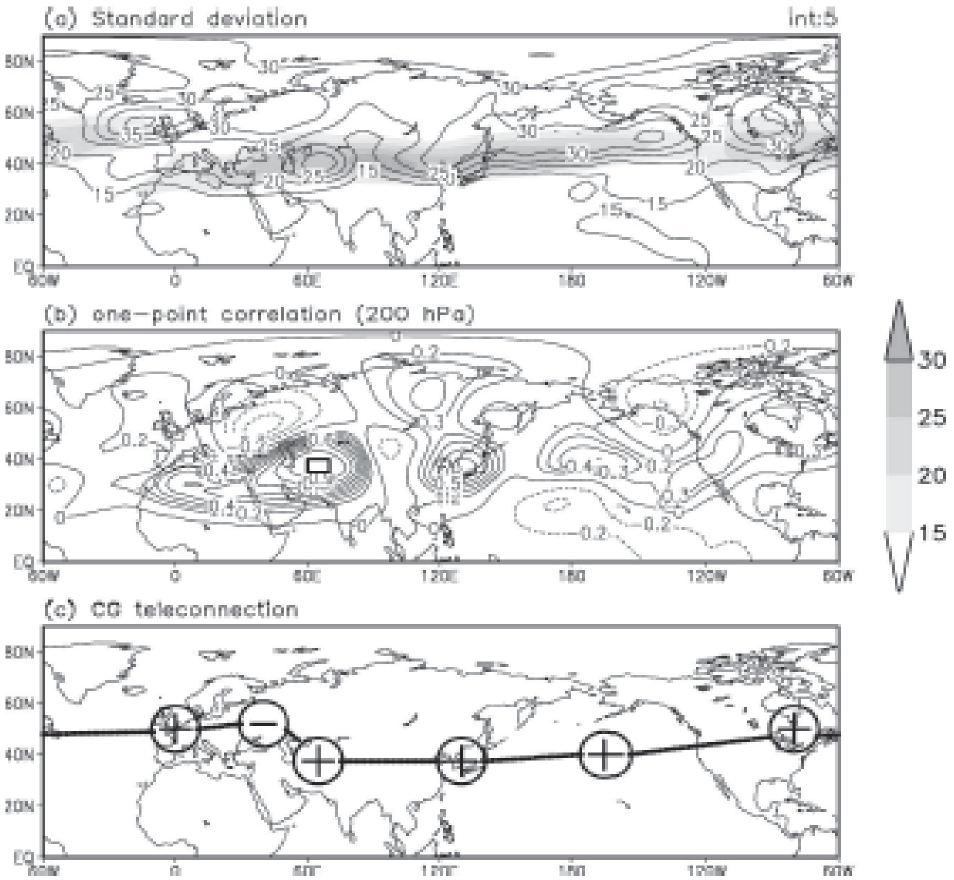

FIG. 1. (a) Standard deviation of summer (JJAS) 200-hPa NH heights (contour) and climatological 200-hPa jet stream (zonal wind) with the magnitude greater than 15 m s^{-1} (shading) for the period of 1948–2003. (b) One-point correlation map between the base-point (box) and summertime (JJAS) 200-hPa geopotential height for 1948–2003. (c) Schematic illustrating six main action centers of the CGT.

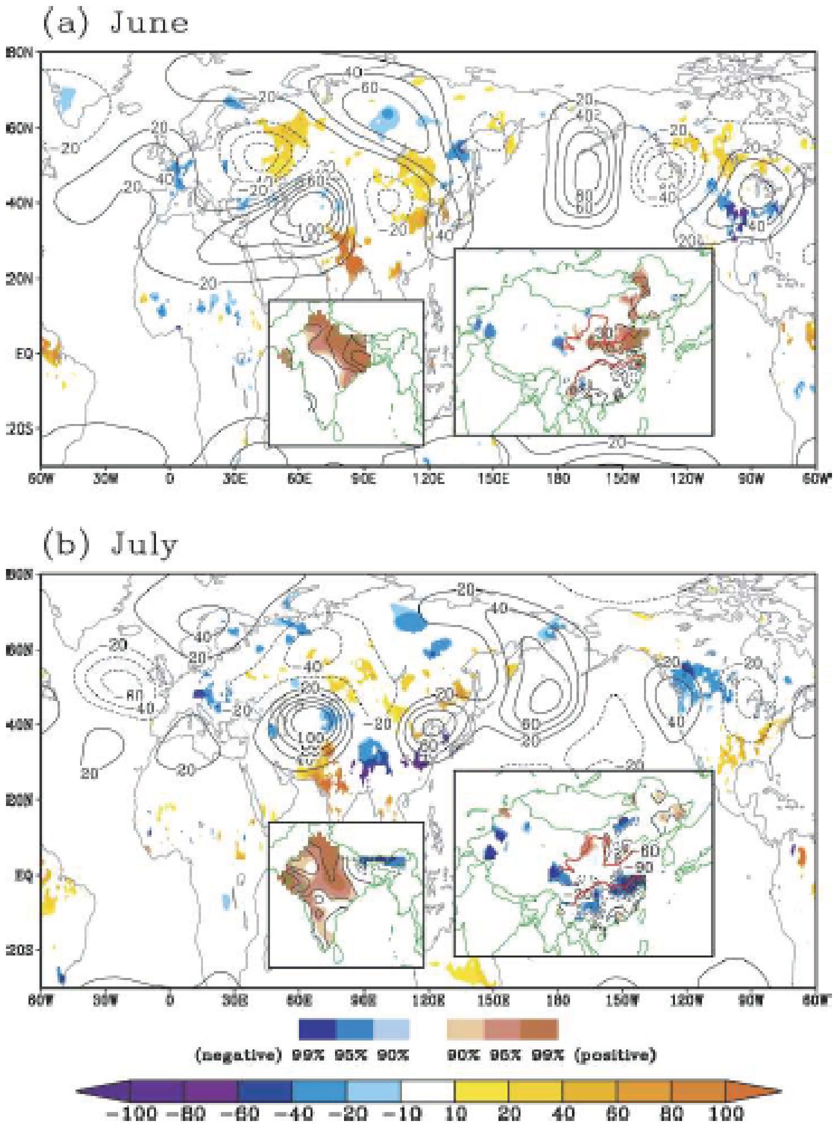

FIG. 7. Composite difference of Delaware global precipitation (background map) and station precipitation (small map) between positive and negative CGTI years for (a) Jun, (b) Jul, (c) Aug, and (d) Sep. Differences (mm month^{-1}) above 90% statistical significance level are shown by shading in global map. The corresponding CGT from Fig. 5 is shown as contour. For India and China station data, red shading denotes regions of difference at 90%, 95%, and 99% confidence levels with a positive value, and blue shading denotes regions of difference at 90%, 95%, and 99% confidence levels with a negative value. Contour intervals are 30 mm month^{-1} (. . . , −60, −30, 30, 60, . . .).

Impact of snow-darkening effect by light absorbing particles on Himalayas-Tibetan-Plateau snowcover, and Asian summer monsoon precipitation

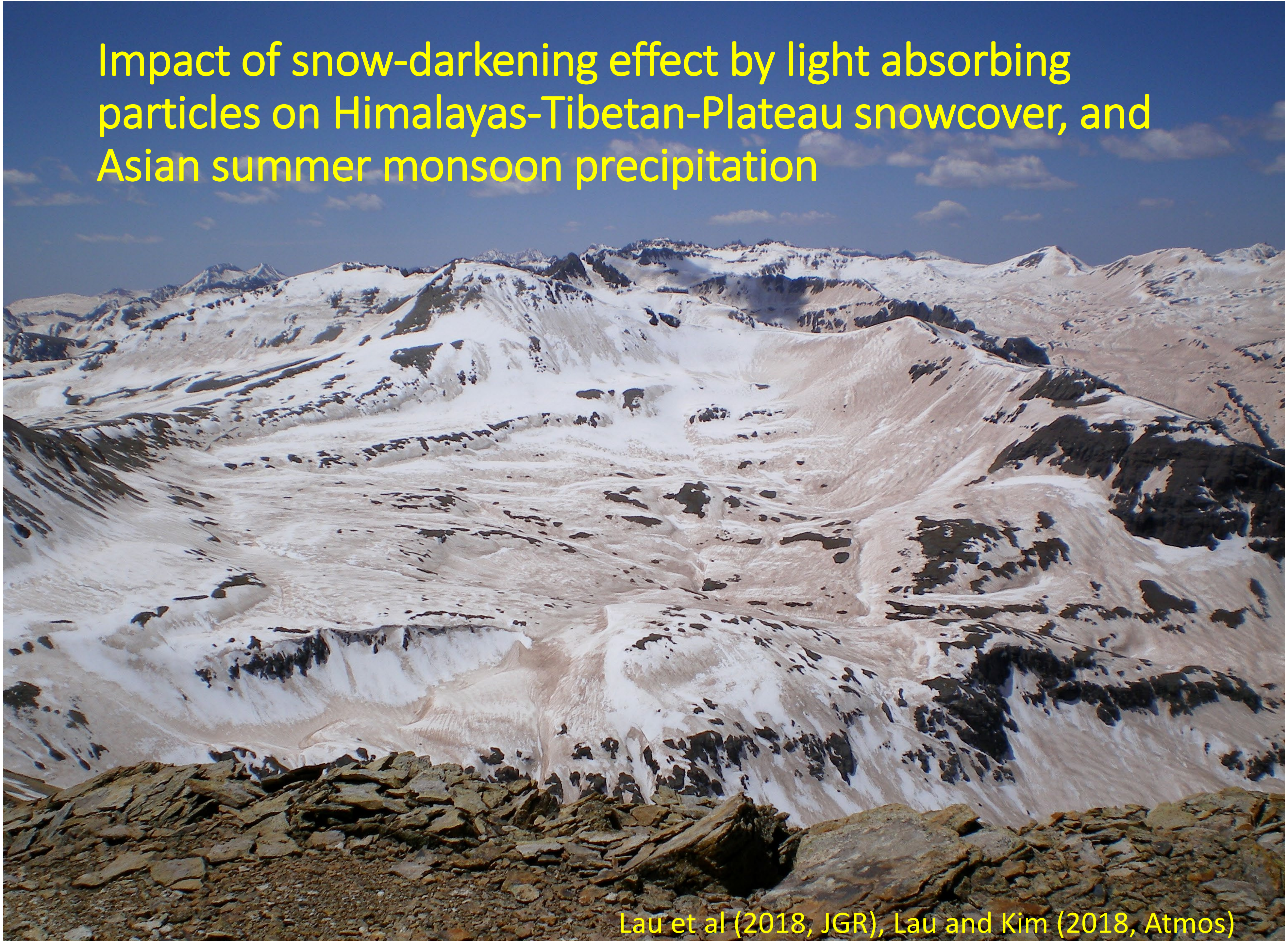

Lau et al (2018, JGR), Lau and Kim (2018, Atmos)

The Elevated Heat Pump (EHP) effect

(Lau et al. 2006, Lau and Kim 2006, Lau et al 2008, 2010, 2017..)

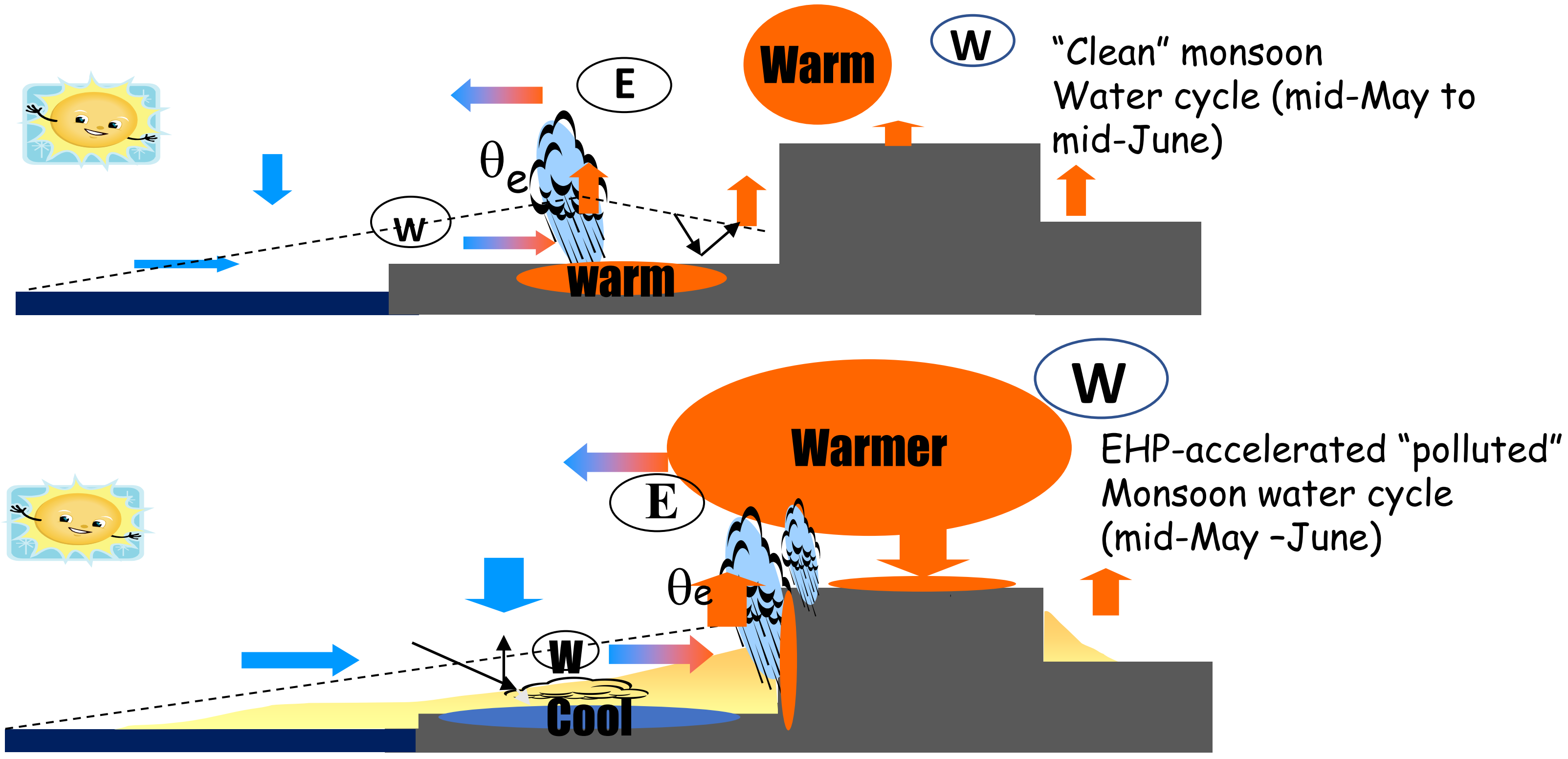

EHP postulates:

a) Enhanced absorbing aerosols warms and moistens tthe upper troposphere over the Tibetan Plateau

b) An advance of the rainy season in northern India/Napal, Himalayas foothills in May-June

c) The increased convection spreads from the foothills of the Himalayas to central India, resulting in an intensification of the Indian monsoon. in June-July

d) Subsequent reduction of monsoon rain in central India in July-August

e) Enhanced transport and deposition of absorbing aerosol (dust, BC and OC) from Middle East and haar desert and Indo-Gangetic Plain , warms the surface increases snowmelt → rapid retreat of Himalayan glacier, providing positive feedback to EHP

Snow Darkening effect (SDE) from NASA/GEOS5 simulation

SDE reduces Surface albedo

Increase land absorption of surface SW radiation

Increases Snow melt

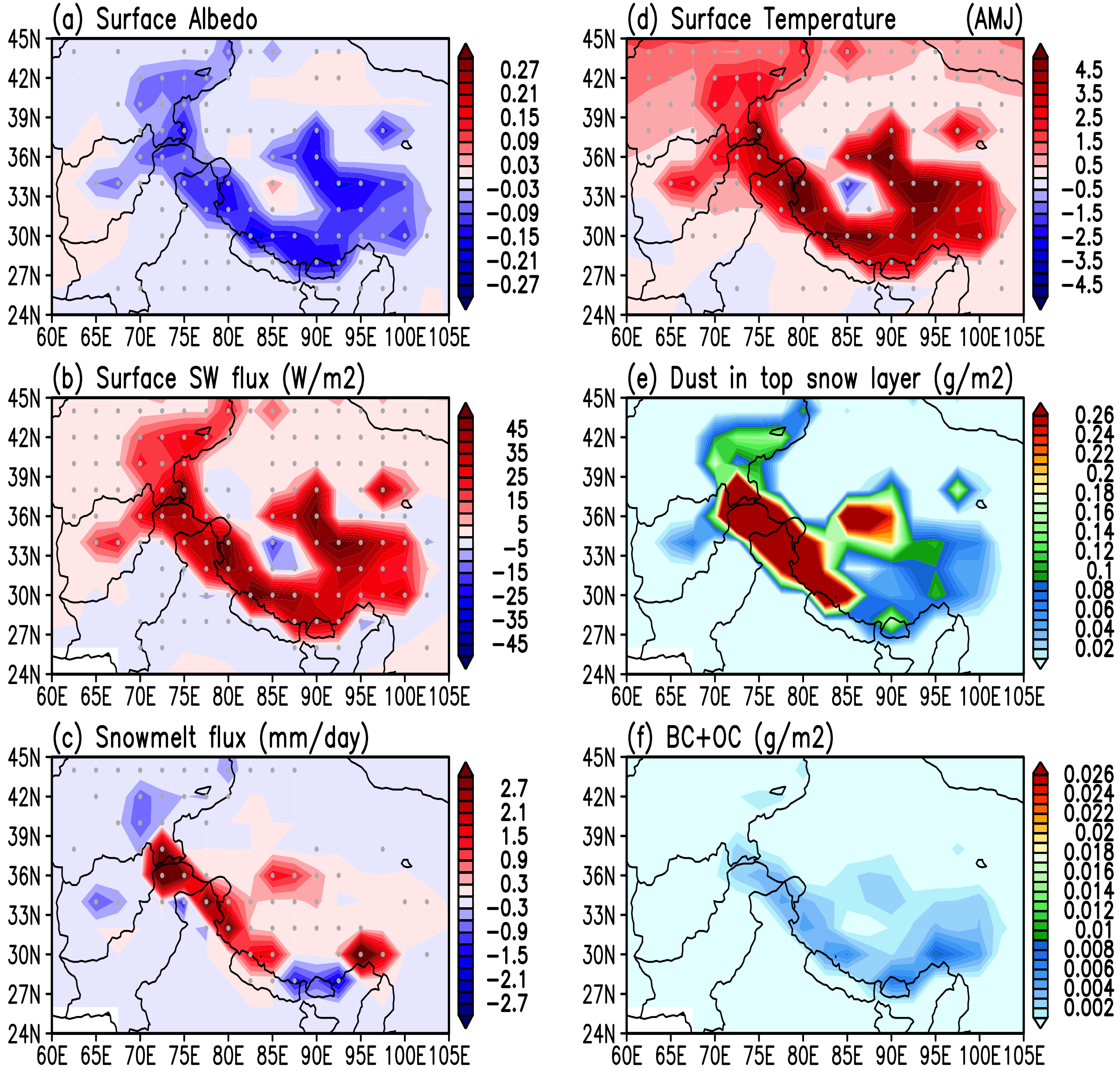

Increased sfc warming of the southern TP Himalayas

Most SDE is due to Dust deposition

BC/OC also contributes

SDE/EHP heating over the TP, excites an upper level Rossby wavetrain

-Warming of HTP and northern Eurasia
-Enhanced Tibetan Plateau Anticyclone
- Subtropical jet weakened shifted north

- Increased precipitation over N. India and HTP regions
- Mei-Yu rain band shifted northward

- MSE/vertical motion forcing centers over the Himalaya slopes and northeastern China

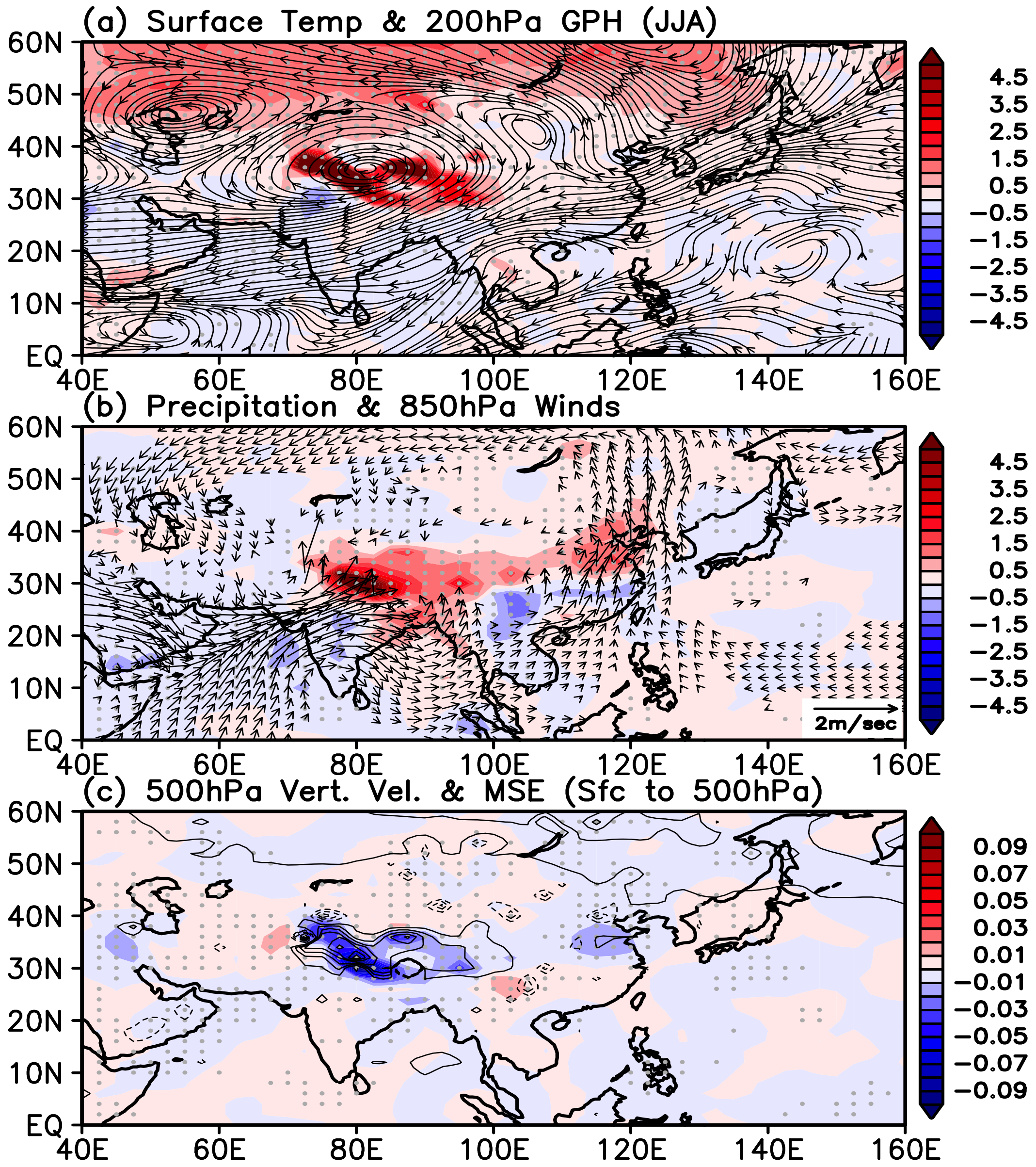

Evolution of SDE of Himalayas/Tibetan Plateau snowcover on the Indian Monsoon (70-90E)

Reduced snow cover | Warming of UT | More dust transport to N.India

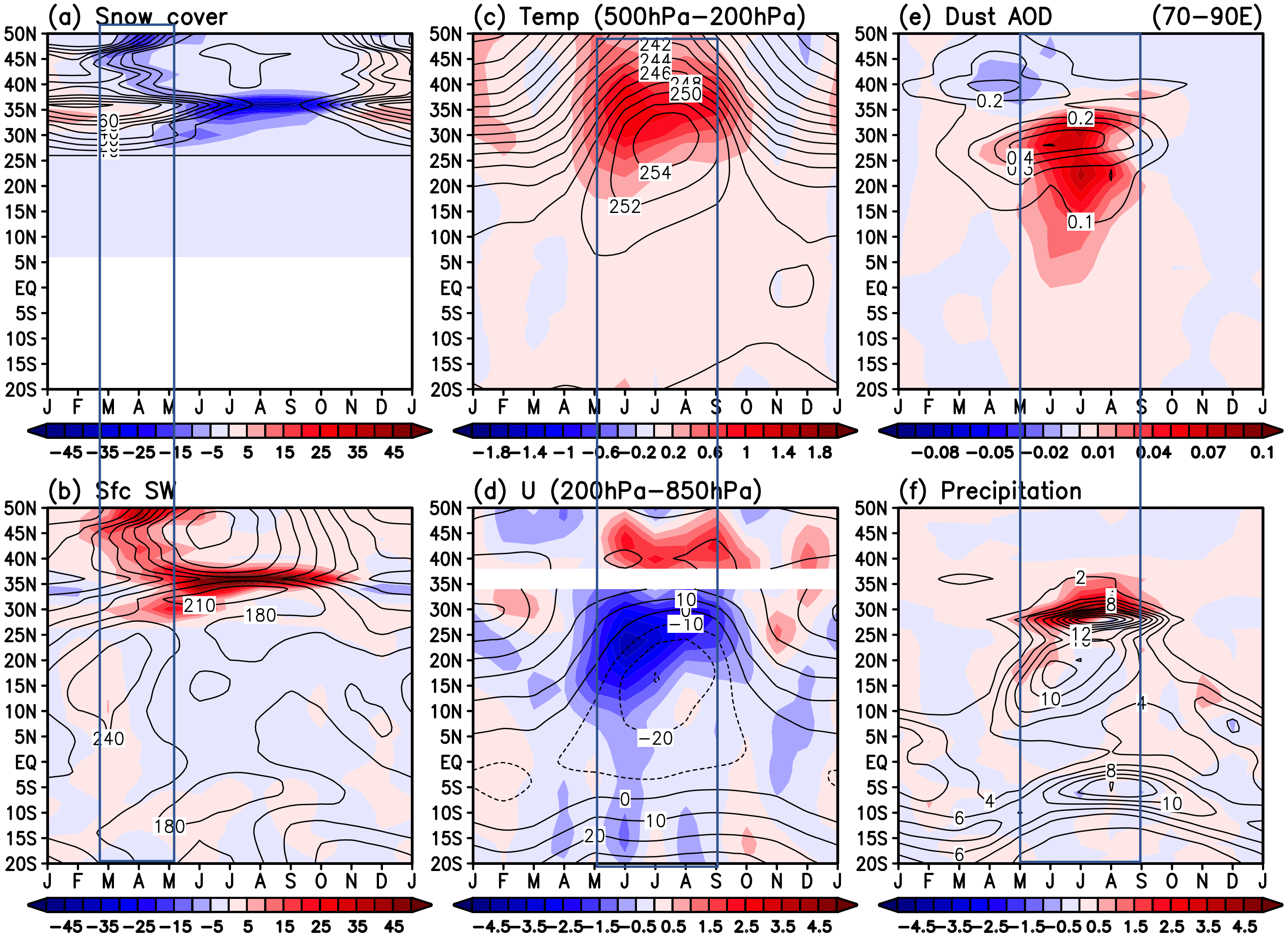

Increased insolation warms Western and southern slopes of TP

Increased tropical upper (lower) easterlies (westerlies)

Stronger monsoon, increased precip over northern India

SDE induced feedback processes in April-May strongly affect Asian summer monsoon precipitation in July-August

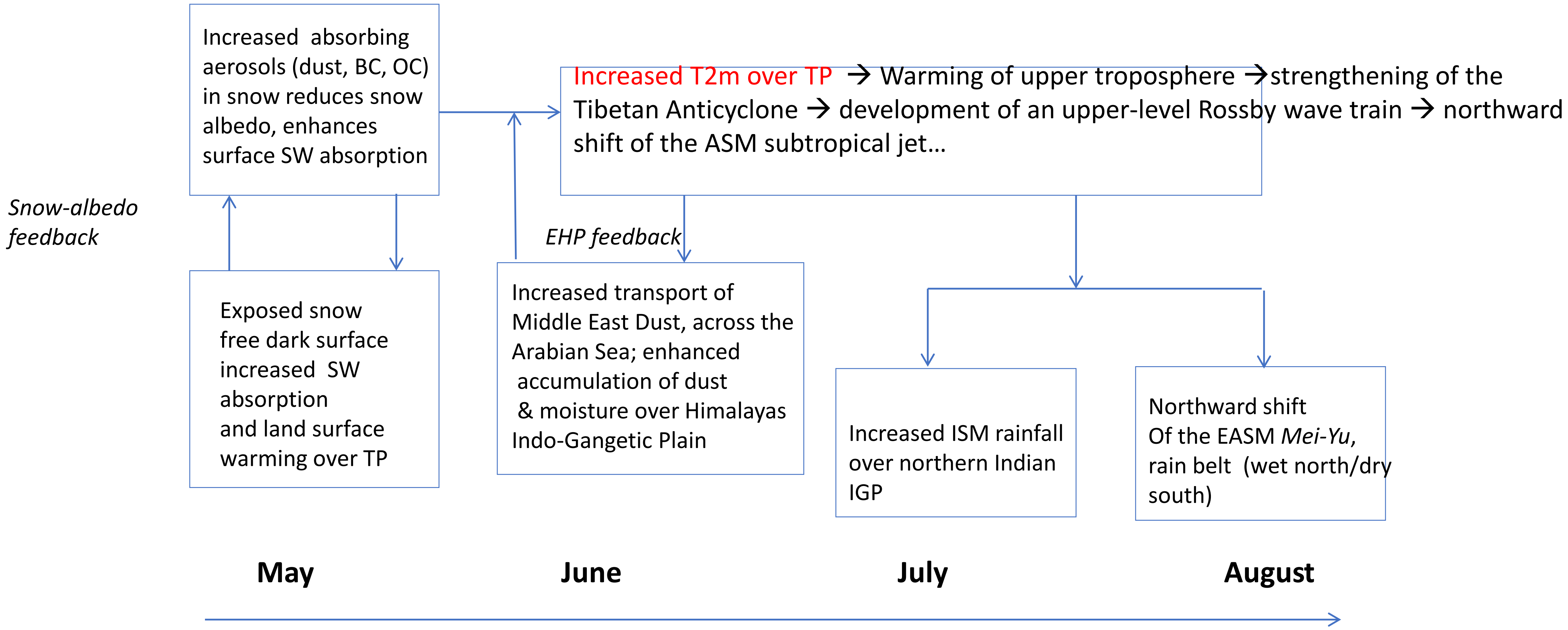

Warming/Cooling of TP excites circum-global teleconnection, enhancing S2S precipitation in US and other regions around the globe → the LS4P project

End

An Aerosol-Monsoon Climate System - A New Paradigm

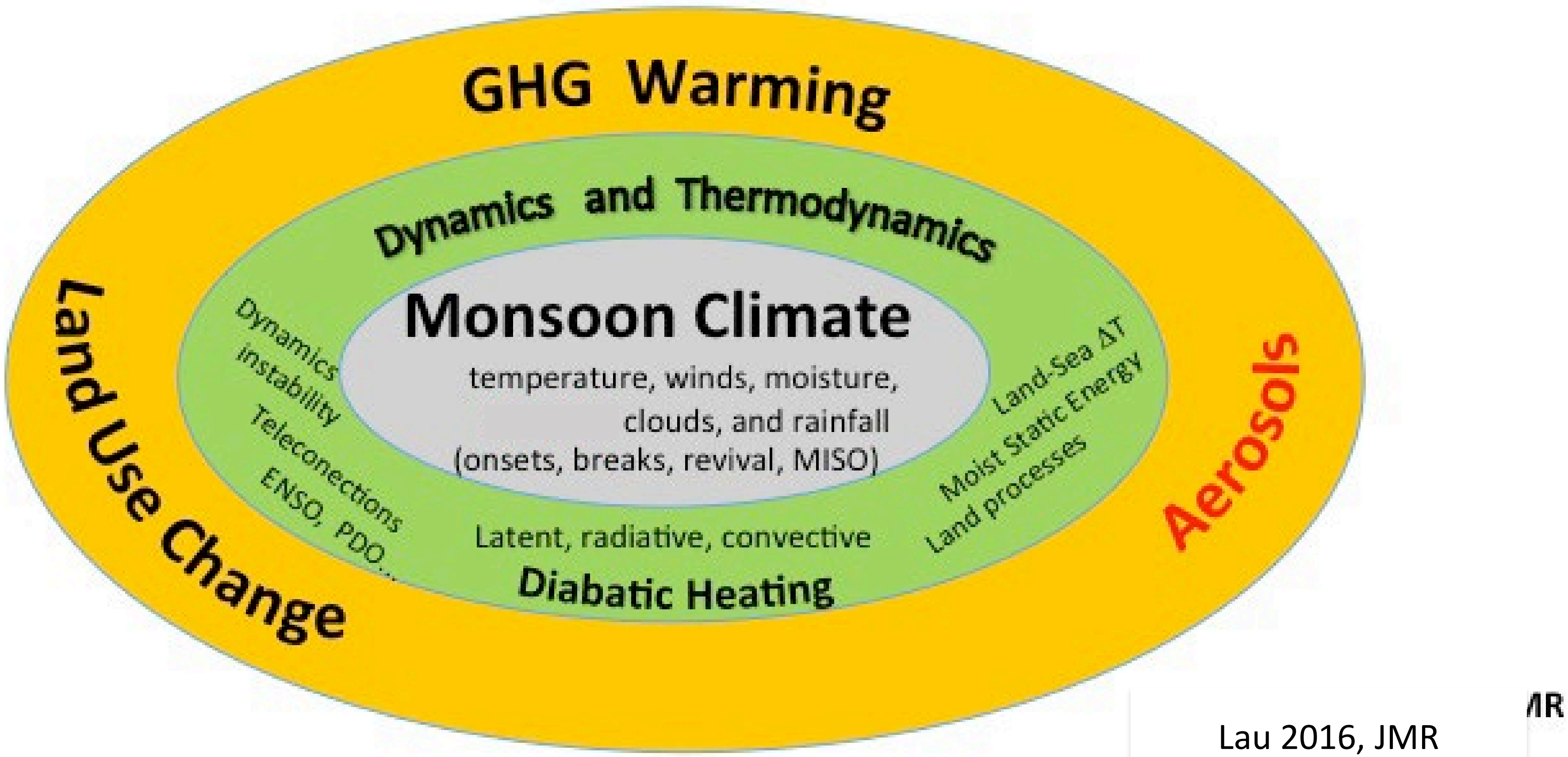

Lau 2016, JMR

The Elevated Heat Pump Hypothesis

(Lau et al. 2006, Lau and Kim 2006, Lau et al. 2008)

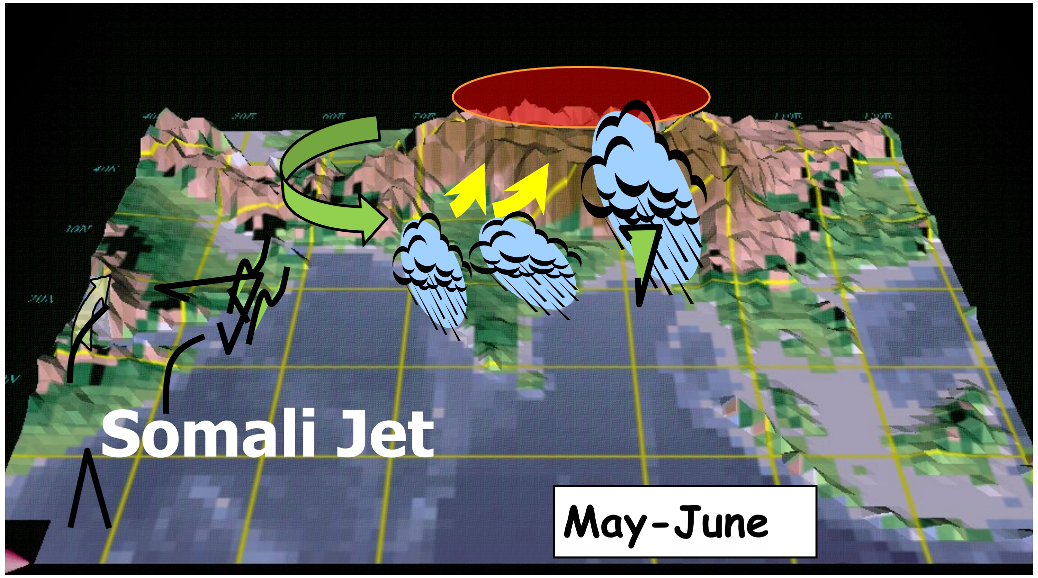

"Clean" Monsoon

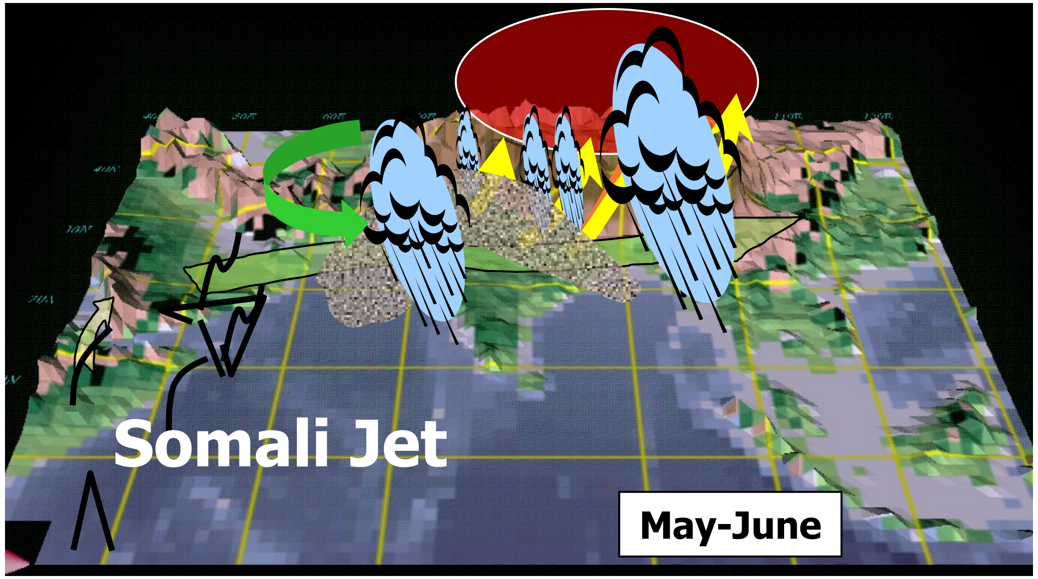

"Polluted" (dust and BC) monsoon

Snow-darkening effect (SDE) on (SDE minus NSDE GEOS5 simulations) Himalayas/Tibetan Plateau snowcover and Asian Monsoon Rainfall

dust deposition on snow

BC deposition

OC deposition

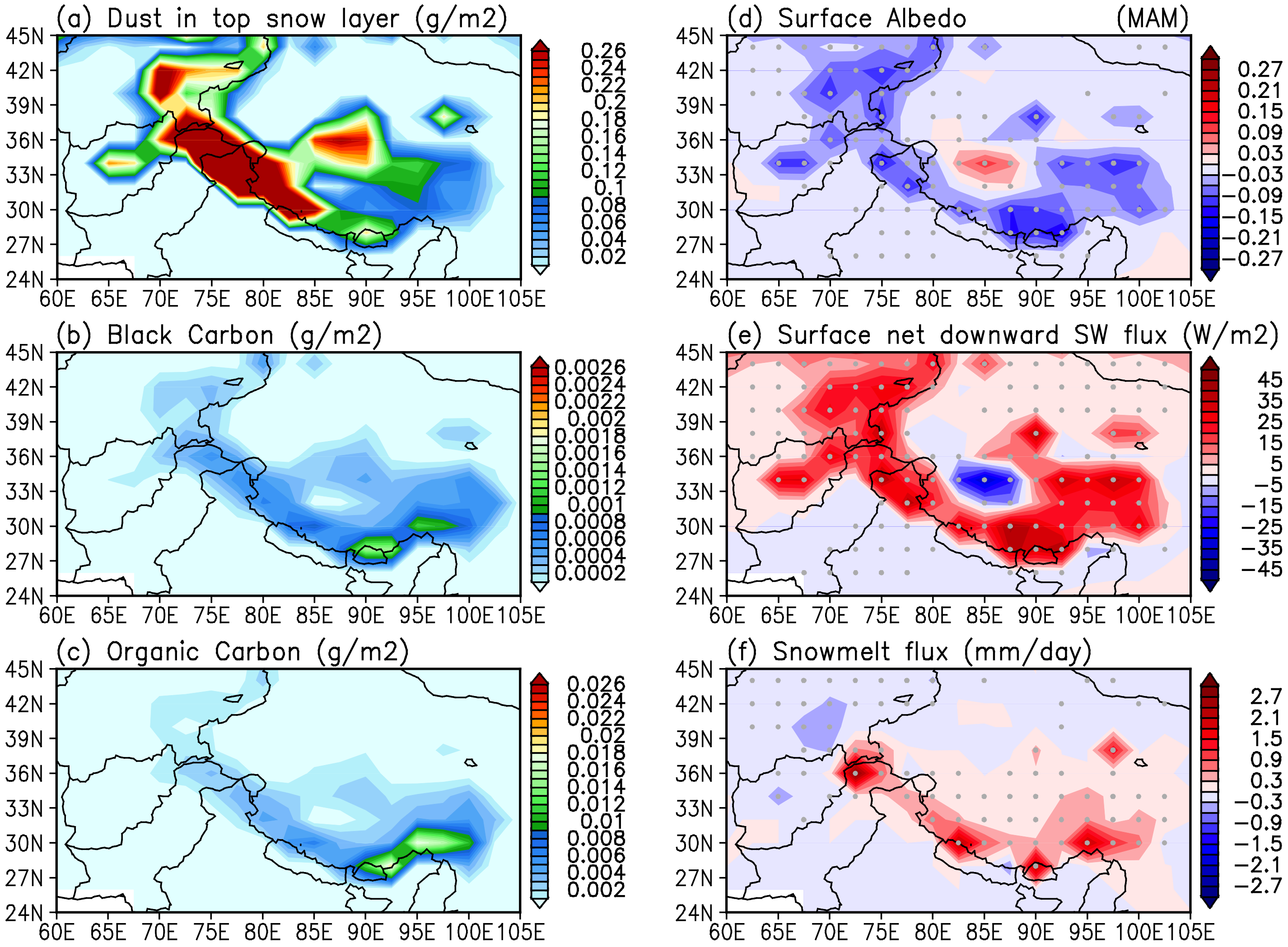

Darkens snow surface
Reduced sfc abledo

Increased surface absorption of downward solar radiation
→ surface warming

Increased snowmelt